HHS Public Access

Author manuscript

Mater Sci Eng C Mater Biol Appl. Author manuscript; available in PMC 2019 December 01.

Published in final edited form as:

Mater Sci Eng C Mater Biol Appl. 2018 December 01; 93: 931–943. doi:10.1016/j.msec.2018.08.060.

Antibacterial dental adhesive resins containing nitrogen-doped titanium dioxide nanoparticles

Fernando Luis Esteban Florez[a], **Rochelle Denise Hiers**[a], **Preston Larson**[b], **Matthew Johnson**[c], **Edgar O'Rear**[d], **Adam J. Rondinone**[e], and **Sharukh Soli Khajotia**[a]

[a)]Department of Dental Materials College of Dentistry, The University of Oklahoma Health Sciences Center, 1201 North Stonewall Avenue, Room 146. Oklahoma City, Oklahoma, 73117, U.S.A.

[b)]The University of Oklahoma, Samuel Roberts Noble Microscopy Laboratory, 770 Van Vleet Oval. Norman, Oklahoma, 73019, U.S.A.

[c)]The University of Oklahoma, Department of Physics and Astronomy, 440 West Brooks Street, Room 129. Norman Oklahoma, 73019, U.S.A.

[d)]The University of Oklahoma, School of Chemical, Biological and Materials Engineering, 100 East Boyd, T-301, Sarkeys Energy Center. Norman, Oklahoma, 73019, U.S.A.

[e)]Oak Ridge National Laboratory, Center for Nanophase Materials Sciences, Oak Ridge, Tennessee, 37831, U.S.A.

Abstract

The development of dental adhesive resins with long-lasting antibacterial properties is a possible solution to overcome the problem of secondary caries in modern adhesive dentistry.

Objectives: Synthesis and characterization of nitrogen-doped titanium dioxide nanoparticles (N_TiO_2), (ii) topographical, compositional and wettability characterization of thin-films (unaltered and experimental) and, (iii) antibacterial efficacy of N_TiO_2-containing dental adhesives against *Streptococcus mutans* biofilms.

Materials and methods: Nanoparticles were synthesized and characterized using different techniques. Specimens (diameter= 12 mm, thickness ≅ 15 μm) of OptiBond Solo Plus (Kerr Corp., USA) and experimental adhesives [50, 67 and 80% (v/v)] were fabricated, photopolymerized (1000 mW/cm^2, 1 min) and UV-sterilized (254 nm, 800,000 μJ/cm^2) for microscopy, spectroscopy, wettability and antibacterial testing. Wettability was assessed with a contact angle goniometer by dispensing water droplets (2 μL) onto four random locations of each specimen (16 drops/group). Drop profiles were recorded (1 min, 25 frames/sec, 37°C) and contact angles were calculated at time=0s ($\theta_{INITIAL}$) and time=59s (θ_{FINAL}). Antibacterial testing was performed by growing *S.*

Corresponding author: Fernando Luis Esteban Florez, fernando-esteban-florez@ouhsc.edu, Phone: +1(405) 271-6545; Fax: +1(405) 271-2902, Department of Restorative Sciences Division of Dental Biomaterials College of Dentistry, 1201 North Stonewall Avenue, Room 146. Oklahoma City, Oklahoma, 73117, U.S.A.

Disclosures:

The authors listed in the present work would like to disclose that the present research is original, it is not being considered for publication elsewhere and that no conflict of interests is associated with the present work. In addition, the authors would like to disclose that they gave their final approval for the manuscript submitted.

mutans (UA159-ldh, JM10) biofilms for either 3 or 24 hours (anaerobic conditions, 37°C) with or without continuous light irradiation (410 ± 10 nm, 3h= 38.75 J/cm^2, 24h= 310.07 J/cm^2) against the surfaces of sterile specimens.

Results: N_TiO_2 was successfully prepared using solvothermal methods. Doped-nanoparticles displayed higher light absorption levels when compared to undoped titania. Experimental adhesives demonstrated superior antibacterial efficacy in dark conditions.

Conclusions: The findings presented herein suggest that N_TiO_2 is a feasible antibacterial agent against cariogenic biofilms.

Keywords

Antibacterial; Nanoparticles; Photocatalysis; Adhesive resins; *Streptococcus mutans*

1. Introduction

Dental caries is one of the most common and costly bacterial infections affecting human beings [1–3]. It is estimated that the treatment of oral biofilm-related diseases costs approximately $81 billion in the U.S. alone [4, 5]. Secondary or recurrent caries is defined as the development of carious lesions at the interface between the adhesive resin and tooth structure [6, 7]. Several studies have shown that secondary caries is the most common cause of failure of dental restorations [8–13]. According to Melo et al. (2013) [3], "*the replacement of failed restorations accounts for around 60% of all restorations performed in the USA each year at an annual cost of over $5 billion*".

The problem of failed restorations is exacerbated on composite resins because these materials have shorter service lives and tend to accumulate more biofilms when compared to enamel [14] and other restorative materials [15]. Hansel et al. [16] while studying the effects of extractable components of composite resins over the growth of oral microorganisms, demonstrated that some co-monomers, such as EGDMA (ethylene glycol dimethacrylate) and TEGDMA (triethylene glycol dimethacrylate), upregulate the growth of acidogenic microorganisms such as *Streptococcus mutans.* It is believed that material-driven artificial selection of acidogenic and aciduric microorganisms [17–20] play important roles in the degradation of a material's surface, adhesive layer deterioration and pulpal irritation. In this context, it becomes critically relevant to develop novel restorative dental biomaterials. Ideally, these novel materials should display superior levels of biocompatibility, promote the deposition of a hydroxyapatite-like layer at the adhesive interface, be acid resistant and should have self-healing, self-cleaning and antibacterial properties.

Previous studies have investigated the antibacterial properties of experimental resin-based restorative materials containing antibacterial agents such as fluoride (F^-) [21], chlorhexidine [22–25], quaternary ammonium dimethacrylate (QADM) [26], 12-methacryloyloxydodecylpyridinium bromide (MDPB) [27], silver nanoparticles (nAg) [28, 29], zinc oxide (ZnO) [30–32] and titanium dioxide nanoparticles (nTiO_2) [33–36] against several oral microorganisms. In 1985, Matsunaga et al. [37] published the first description of the photochemical sterilization of *Lactobacillus acidophilus*, *Saccharomyces cerevisiae* and

Escherichia coli using titanium dioxide (TiO_2) powders with halide lamp irradiation (60–120 min). The fundamental mechanism of TiO_2 photocatalysis is based on the interaction of light, at appropriate wavelength and photon energy with the surface of the photocatalyst. If such electronic requirement is satisfied (i.e. 385 nm and 3.2204 eV for anatase), then electrons pertaining to the valence band (fundamental state) will be promoted into the conduction band (excited state) leaving a positively charged electron vacancy in the valence band.

The resulting free electrons of the conduction band (e^-_{CB}) and the positively charged holes (h^+_{VB}) of the valence band (Equation 1) [38] may recombine to release the excess energy in the form of heat or light [39]. If recombination doesn't occur, newly generated e^-_{CB} and h^+_{VB} migrate to the photocatalyst's surface to participate in numerous oxidation and reduction reactions. These reactions will then generate reactive oxygen species (ROS), as described in equations 2 and 3. Follow-on reactions (Equations 4–7) can generate hydrogen peroxide (H_2O_2) or hydroperoxyl radicals (•OOH) [38].

$$TiO_2 + hv \rightarrow e^-_{CB} + h^+_{VB} \quad (1)$$

$$H_2O + \quad h^+_{VB} \quad \rightarrow \quad \cdot OH + \quad H^+ \quad (2)$$

$$OH^- + \quad h^+_{VB} \quad \rightarrow \quad \cdot OH \quad (3)$$

$$2 \quad O_2^{\cdot -} + 2H^+ \rightarrow H_2O_2 + O_2 \quad (4)$$

$$\cdot OH + \quad \cdot OH \quad \rightarrow \quad H_2O_2 \quad (5)$$

$$O_2^{\cdot -} + \quad H_2O_2 \rightarrow \quad \cdot OH + OH^- + O_2 \quad (6)$$

$$O_2^{\cdot -} + H^+ \rightarrow \cdot OOH \quad (7)$$

Despite its proven efficacy against microorganisms relevant to public health, the underlying antibacterial mechanism of TiO_2 photocatalysis remains to be fully elucidated. It is believed

that ROS generated due to TiO_2 irradiation will preferentially attack polyunsaturated phospholipids of the microorganisms' membranes by a lipid peroxidation process [40, 41]. This process causes a chain reaction that promotes the denaturation of proteins and electron mediators. The progression of this process leads to complete membrane disruption, cytoplasm leakage and cell death. However, even though TiO_2 photocatalysis is a conceptually feasible technology [42], its efficacy is dependent on the use of UV irradiation at energy levels extremely dangerous to human cells and tissues [43]. Nevertheless, Cai et al. [33–36, 44] have demonstrated the successful incorporation of 5–30% of $nTiO_2$ in dental adhesive resins. Their findings demonstrated that experimental adhesive resins displayed antibacterial and bioactive properties when irradiated with UVA (371 nm) along with energy doses that ranged from 3 to 43 J/cm^2 which, in dermatological applications are considered as moderate-to-high energy doses [45].

Recent advancements have focused on strategies to narrow the TiO_2 band gap to facilitate visible light absorption and overcome the necessity to use UV wavelengths (100–400 nm). In this direction, Asahi et al. (2001) [46] using the full-potential linearized augmented plane wave (FLAPW), have calculated the density of states (DOSs) of substitutional doping with non-metal ions (N, C, F, P and S) for oxygen (O) in the anatase crystalline structure. Their findings demonstrated that doping with nitrogen produced materials with superior visible photocatalytic activity because nitrogen introduces a midgap state (N 2p, ≈ 2.47 eV) located above the regular valence band of TiO_2 (O 2p, ≈ 3.2 eV for anatase) [47]. As a result, the band-gap narrows and allows for the photo-excitation of electrons with the use of visible wavelengths (400–700 nm).

Therefore, the objectives of the present study were: (i) Synthesis and characterization of nitrogen-doped titanium dioxide nanoparticles (N_TiO_2) in a form compatible with dental adhesive resins, (ii) topographical, compositional and wettability analyses of thin-films fabricated with unaltered or N_TiO_2-containing dental adhesive resins and (iii) determination of the antibacterial efficacy of N_TiO_2 immobilized in experimental dental adhesive resins against *Streptococcus mutans* biofilms.

2. Materials and Methods

2.1 Synthesis of N_TiO_2

Nitrogen-doped TiO_2 nanoparticles were synthesized via a 2-step process. The first step was the solvothermal synthesis of pure TiO_2 in a manner similar to Dinh et al. [48]. The second step was nitrogen-doping of the TiO_2 in a manner similar to Huo et al. [49]. In a typical reaction, a solution comprised of 1.7 g of Ti(IV)-butoxide (Aldrich, 97 %), 4.6 g ethanol (Decon Labs, 200 proof), 6.8 g oleylamine (Aldrich, 70 %), and 7.1 g oleic acid (Aldrich, 90%) was prepared, then mixed with 20 mL of 4% H_2O in ethanol (18-MΩ Milli-Q; Decon Labs). Each solution was clear before mixing, but the final mixture immediately clouded due to formation of micelles and likely some hydrolysis. This solution was then split into two portions (around 20 mL/portion), and each portion was placed into a high-pressure reaction vessel (Paar Series 5000 Multiple Reactor System) and reacted at 180°C for 24 hours. The vessels were stirred via external magnetic field and Teflon-coated stir bars. The reaction vessels were Teflon-lined. Upon cooling, the solutions were decanted and rinsed 3 times

with anhydrous ethanol to remove extraneous surfactants. The pure TiO_2 nanoparticles were readily dispersible into 20–30 mL ethanol, but did not form clear solutions. The TiO_2 nanoparticles were stored in ethanol.

For the second step, a portion of the TiO_2 nanoparticles in ethanol were then reacted with an equal volume of triethylamine (Aldrich, 99.5 %), also using the high-pressure reaction vessel, at 140°C for 12 hours. The exact concentration of TiO_2 in ethanol/triethylamine varied, but in every instance, there was a large excess of triethylamine. Upon cooling, the now-doped N_TiO_2 particles were rinsed 3 times with anhydrous ethanol. The final N_TiO_2 nanoparticle solution was in ethanol, and the concentration of particles was determined gravimetrically and was approximately 35 mg/mL.

2.2 Characterization of N_TiO_2

2.2.1 UV-VIS spectroscopy—TiO_2 (P25, Evonik Degussa GmbH, Germany) and N_TiO_2 (Oak Ridge National Laboratory, USA) nanoparticles in ethanol suspension were individually characterized in terms of optical absorbance with a Cary®50 (Agilent Technologies, Santa Clara, CA) spectrophotometer using the transmittance method. Aliquots (20 μL) of each material (either P25 or N_TiO_2, 40 mg/mL in ethanol) were individually placed in a quartz microcell. Each sample was then placed inside the spectrophotometer's chamber between the light source and the photodetector, and the intensity of light that reached the photodetector was measured from 190–900 nm in 2 nm increments.

2.2.2 Scanning Electron Microscopy (SEM)—Aliquots (5 μL) of N_TiO_2 suspended in ethanol in the as-synthesized concentration (200 proof, 40 mg/mL, Oak Ridge National Laboratory, USA) were placed onto a polished silicon wafer. N_TiO_2 samples were air-dried in room temperature until all the solvent had been evaporated. Individual N_TiO_2 samples were then mounted onto standard aluminum SEM pin stubs (diameter 1/8") and were sputter coated with a thin-layer (~4 nm) of iridium using a sputter coater (K575D, Emitech Sample Preparation, UK) prior to the imaging process. Adhesive specimens containing 50, 67 and 80 % (v/v) were mounted directly onto standard aluminum SEM pin stubs using double-sided carbon tape and silver paste for electrical grounding to the stub. The adhesive samples were sputter coated using the same procedures described for the N_TiO_2 in suspension. Both, N_TiO_2 in suspension and immobilized in dental adhesive resins were imaged using a Zeiss Neon 40 EsB SEM at 5 kV. Energy dispersive X-ray spectroscopy (EDS) and EDS compositional mapping was performed using an Oxford INCA 250 microanalysis system with an analytical drift detector at 15 kV.

2.2.3 Transmission electron microscopy (TEM)—Nitrogen-doped TiO_2 nanoparticles suspended in ethanol (200 proof, 0.032 mg/mL, Oak Ridge National Laboratory, USA) were dispersed by brief sonication in an ultrasound bath (Bransonic 220, Branson Ultrasonics, USA). A drop of suspended TiO_2 nanoparticles was placed on holey carbon coated copper grids. The drop was allowed to adsorb for 1–2 min, then wicked with filter paper to remove excess fluid, and dried before viewing in a JEOL 2000FX transmission electron microscope. Images were made on Carestream® Kodak® electron image film SO-163 (Eastman Kodak Company, USA) and digitized with an Epson

Perfection V750-M Pro scanner (Epson America, Inc. USA). X-ray spectra were collected using a Kevex thin window detector and EDS software (IXRF Systems Inc., USA)

2.3 Specimen fabrication

Disk shaped specimens (diameter= 12.00 mm, thickness≅ 15 μm) of OptiBond Solo Plus adhesive resin (Kerr Corp., USA) and experimental adhesive resins containing 50, 67 and 80 % (v/v) of N_TiO_2, were manually fabricated by individually dispensing 10 μL of each material onto the surfaces of separated glass coverslips (No.2, VWR International, LLC). Both the unaltered and experimental adhesive resins were then uniformly spread over glass coverslips using disposable flexible applicators (Kerr Corp., USA) and were polymerized using blue light irradiation (1000 mW/cm^2, 1 min) emitted from a broadband LED light-curing unit (VALO, Ultradent Products, Inc., USA). Specimens of both unaltered and experimental adhesive resins were then UV-sterilized (254 nm, 800,000 μJ/cm^2, UVP Crosslinker, model CL-1000, UVP, USA).

2.4 Bacterial Strain

Streptococcus mutans strain UA159 (JM10 : : pJM1-ldh, luc+, Spc^R, *luc* under the control of the *ldh* promoter) was utilized for this project. The selection of antibiotic-resistant colonies was performed on TH plates (Todd-Hewitt, BD Difco, USA) supplemented with 0.3 % yeast extract (EMB, Germany) and 800 μg/mL of spectinomycin (MP Biomedicals, USA). The plates were incubated under anaerobic conditions at 37°C for 48 h.

2.5 Antibacterial behavior of N_TiO_2 immobilized in dental adhesive resins

In order to assess the antibacterial efficacy of experimental adhesive resins containing 50, 67 and 80 % (v/v) of N_TiO_2 (Oak Ridge National Laboratory, USA), *S. mutans* biofilms were grown against the surfaces of sterile specimens of both unaltered and experimental adhesive resins. Planktonic cultures of *S. mutans* (UA159-ldh, JM10) were grown in THY culture medium at 37°C for 16 hours. Planktonic cultures having optical density (OD_{600}) levels ≥ 0.900 were used as inoculum to grow the biofilms. A 1:500 dilution of the inoculum was added to 0.65× THY + 0.1 % (w/v) sucrose biofilm growth medium. Aliquots of inoculated biofilm growth media (2.5 mL) were dispensed into the wells of sterile 24-well microtiter plates (Falcon, Corning, USA) containing sterile specimens. Biofilms were grown for either 3 or 24 hours (static cultures, anaerobic conditions, 37°C) with or without continuous light irradiation provided by a prototype LED device (410 ± 10 nm, 3h irradiation= 38.75 J/cm^2, 24h irradiation= 310.07 J/cm^2).

After the growth period, biofilms were replenished with 2.5 mL of fresh 1× THY + 1 % (w/v) glucose culture medium and were incubated at 37°C for 1 hour. Replenished biofilms were transferred into individual sterile polypropylene tubes (3.0 mL, ConSert Vials, Thermo Fisher Scientific, USA) containing 1.0 mL of fresh 0.65× THY + 0.1 % (w/v) sucrose medium. Vials containing the specimens were sonicated to facilitate the removal of the adherent biomass using a sonicator (Q700 sonicator, QSonica, USA) connected to a water bath (4°C; 4 cycles of 1 minute, 15 second interval between cycles; power 230 ± 10 W, total energy≈ 78 kJ).

2.6 Viable colony counts

Biofilms grown on the surfaces of both unaltered and experimental dental adhesive resins (section 2.5) were sonicated to allow the antibacterial efficacy assessment using the colony-forming units method (CFU). The procedures involved in the viable colony counts (CFU/mL) measured in the present study have been described in detail in our previous publication [50], and will be summarized here. Immediately after sonication procedures, inoculum aliquots (10 μL) from each specimen were diluted in 90 μL of 0.65x THY + 0.1 % (w/v) sucrose sterile culture medium. Serial dilutions (10^{-6}) were then carried out in that culture medium for all samples using a multi-channel pipette (5–50 μL, VWR, USA). Aliquots (10 μL) of each dilution were then plated in triplicate (total: 30 μL/sample/dilution) using THY plates supplemented with 800 μg of spectinomycin.

2.7 Staining and Confocal Laser Scanning Microscopy

A separate set of specimens was fabricated as described in section 2.3. Biofilms were then grown on the surfaces of unaltered and experimental adhesive resins, using the same conditions described in section 2.5 in preparation for staining and confocal microscopy. The biofilms on all specimens were stained using BacLight™ LIVE/DEAD fluorescent stains (1.67 μM each of Syto 9 to stain live cells and propidium iodide to stain dead/damaged cells, Molecular Probes, USA) and kept hydrated prior to confocal microscopy. The confocal microscopy procedure has been described in detail in our previous publication [51], and will be summarized here. The full thickness of biofilms on all specimens was imaged at three randomly selected locations per specimen, in order to gain a representative sample for each specimen, using a Leica TCS SP2 MP confocal laser scanning microscope (CLSM) with Ar (488 nm) and He/Ne (543 nm) lasers for excitation of the fluorescent stains. A 63x water immersion microscope objective lens was used and serial optical sections were recorded from the top of the specimen to the top of the biofilm at 0.6 μM intervals in the z-direction. Representative 3-D reconstruction images of live and dead/damaged cells in the 24-hour biofilms grown on adhesive resins were generated using Volocity software (Version 4.4.0, Velocity Software solutions Pvt. Ltd., India) to facilitate visualization of biofilm distribution in all groups investigated.

2.8 Contact angle goniometry

A separate set of specimens (n= 4/group/concentration) was fabricated as described before (section 2.3 above) in preparation for the contact angle goniometry at oral temperature (37°C). Immediately after fabrication, specimens of each group were left undisturbed (10 min) inside the environmental chamber of a contact angle goniometer (OCA15-Plus, Dataphysics Instruments, Germany) for thermal equilibration prior to testing. The wettability of water was tested at oral temperature by displacing a 2 μL drop of ultrapure water onto four random locations of each specimen (16 drops/group). The profiles of the axisymmetric drops were recorded using a high-speed and high-definition CCD camera (1 min, 25 frames/sec). The evolution of drop profiles over time was analyzed using SCA20 software (Dataphysics Instruments, Germany) and the Laplace-Young equation was used to calculate the contact angles at time= 0s ($\theta_{INITIAL}$) and time= 59s (θ_{FINAL}).

2.9 Statistical Analysis

The statistical analyses were performed using the SAS software (version 9.2; SAS Institute, USA). The viable colony counts (CFU/mL) for biofilms grown with or without light irradiation, and the wettability of dental adhesive resins containing varying concentrations of N_TiO_2 (10–80%) were analyzed using General Linear Models (GLM) and Student-Newman-Keuls *post hoc* tests ($\alpha = 0.05$).

3. Results

3.1 UV-vis spectroscopy

Figure 1 represents the UV-vis spectroscopy results for both the undoped and nitrogen-doped titanium dioxide nanoparticles. It is possible to observe that doped samples displayed higher absorption levels throughout the range of wavelengths considered, which confirms that nitrogen was successfully incorporated into the crystal lattice of titania.

3.2 SEM, EDS and TEM characterization of non-immobilized N_TiO_2

Figure 2 represents the SEM pictures of N_TiO_2 nanoparticles at different magnifications (500x to 50,000x). Even though it is possible to observe a strong behavior of nanoparticles agglomeration in the as-synthesized concentration (40 mg/mL in ethanol 200 proof), these pictures suggest that nanoparticles fabricated by the solvothermal method (described in section 2.1) have an approximate spherical shape, smooth surfaces and most of the nanoparticles exhibit some faceting. Figure 3 represents the EDS pictures of the compositional analysis of the N_TiO_2 nanoparticles in the as-synthesized concentration (40 mg/mL). The mapping of elements indicates large quantities of titanium (Ti), oxygen (O), carbon (C) and silicon (Si). The visible peaks present in the EDS compositional spectrum confirm the presence and the relative amounts (in wt %) of the elements in the samples investigated. Figure 4 shows TEM images (500,000x magnification) and compositional analysis of N_TiO_2. The TEM images presented confirm the SEM findings regarding the nanoparticles' morphologies and demonstrated that synthesized nanoparticles had sizes varying around 10 nm. In addition, it is also possible to observe that even for a very diluted sample (1:1250 in absolute ethanol) the nanoparticles still display a tendency to agglomerate.

3.3 SEM and EDS characterization of N_TiO_2 immobilized in dental adhesive resins

Figure 5 represents the SEM pictures images [500x (A, C, E, G) and 5,000x (B, D, F, H) magnifications] of thin-films of both unaltered and experimental dental adhesive resins containing 50, 67 or 80 % (v/v) of N_TiO_2. It is possible to observe (images 5C-5H) that adhesive resins containing higher N_TiO_2 concentrations resulted in materials with rougher surfaces due to the higher presence of particles at the surface level. In addition, it is possible to observe that materials containing 67 and 80 % (v/v) presented particles (images 5E-5H) that were not covered by the adhesive matrix when compared to the remaining groups. This finding can be observed by the presence of circular-shaped particulates of very intense brightness. Figure 6 represents the results of the compositional analysis of both unaltered and experimental dental adhesive resins. It is possible to observe in image 6A that the

elements composing the unaltered adhesive resins were mainly barium, silicon, oxygen and carbon, which is in agreement with the composition expected for the unaltered dental adhesive resin. Images 6B to 6D demonstrate increasing amounts of titanium and oxygen, which can be observed in the images by the presence of increasing amounts of pink (Ti) and yellow dots (O).

3.4 Contact angle goniometry

The results obtained from the assessment of the wettability of water at times 0s ($\theta_{INITIAL}$) and 59s (θ_{FINAL}) on both unaltered and experimental dental adhesive resins are presented in a self-explanatory graph of mean and standard deviation values (Figure 7). The results demonstrate that, independent of the group considered, initial contact angles (t= 0s) had values that were consistently higher than the values of the final contact angles (t= 59s). The SNK *post hoc* test demonstrates that similar initial contact angle values were obtained in all groups tested. Although final contact angles were smaller in value than initial contact angles, a similar trend of wettability behavior could still be noticed, where no significant differences could be observed among the groups tested.

3.5 Antibacterial behavior of N_TiO_2 immobilized in dental adhesive resins

The results of the antibacterial efficacy of N_TiO_2 immobilized in dental adhesive resins against 3 or 24-hour *S. mutans* biofilms grown against the surfaces of specimens of both unaltered and experimental dental adhesive resins (section 2.5) under dark or continuous light irradiation conditions were determined using viable colony counts (section 2.6) and are presented in self-explanatory graphs (Figures 8 and 9) of mean and standard deviation values (CFU/mL). The results presented indicate that independently of the experimental groups tested or periods of time considered (either 3 or 24-hour), biofilms grown under continuous light irradiation conditions (410 ±10 nm, 3h irradiation= 38.75 J/cm^2, 24h irradiation= 310.07 J/cm^2) displayed lower viability levels when compared to biofilms pertaining to either the control group or to experimental groups where biofilms were grown without light irradiation. It is also possible to observe that biofilms grown under continuous light irradiation displayed similar viability levels independent of the material investigated. In addition, the results of the viability levels of biofilms grown in dark conditions suggest that experimental adhesive resins may also have antibacterial properties that are not dependent on light irradiation.

3.6 Confocal Laser Scanning Microscopy

The CLSM analysis of 24-hour *S. mutans* biofilms grown on the surfaces of both unaltered and experimental dental adhesive resins are presented in figure 10 (images 10A-10H). The 3D renderings revealed that the morphology, biovolume and viability of the cells within the investigated biofilms were significantly altered based on N_TiO_2 concentrations (50, 67 and 80 % [v/v]) and light irradiation conditions (with or without). The results presented have clearly demonstrated that independent of the experimental group considered, all biofilms grown under continuous light irradiation conditions (images 10B, 10D, 10F and 10H) expressed higher instances of red fluorescence, which denotes that these biofilms had lower viability levels than the biofilms grown in dark conditions, which predominantly fluoresced green (images 10A, 10C, 10E and 10G).

These findings demonstrate that the wavelength and dose of energy used (410 ±10 nm, 3h irradiation= 38.75 J/cm^2, 24h irradiation= 310.07 J/cm^2) during the growth of biofilms significantly impacted the ability of *S. mutans* to sustain viable biofilms. It is also noticeable in the CLSM results that the combination of continuous-light irradiation and experimental materials with higher nanoparticles concentrations (67 and 80 %) supported biofilms displaying the least amount of biovolume and viability, which can be noted on the images by the presence of extremely sparse micro colonies displaying intense red colors (images 10F and 10H). The results obtained for biofilms pertaining to non-irradiated groups indicate that experimental materials containing 50, 67 and 80 % (v/v) of N_TiO_2 in dark conditions displayed antibacterial properties that were not dependent on light irradiation and further confirm the CFU/mL results. This finding can be observed specially on the images 10E and 10G as colonies displaying colors that are a mix of red, green and yellow. In addition, it is also possible to observe that biofilms grown under dark conditions produced biofilms of similar biovolume and thickness, as noted by the large chained amorphous colonies (images 10A, 10C, 10E and 10G) regardless of group parameters. This finding indicates that the amounts of dead colonies present on the images are directly proportional to increasing amounts of the N_TiO_2 in the materials investigated.

3. Discussion

TiO_2 has proven to be the most widely used semiconductor metal-oxide photocatalyst due to its strong oxidizing effect, biocompatibility, long-term photostability and low cost. In addition, pure TiO_2 photocatalyst are widely known to be effective agents against Gram-positive and Gram-negative bacteria upon UV irradiation [33–36, 38]. However, the UV energy doses required to promote adequate sterilization are at levels extremely dangerous to human cells and tissues [43], thus restraining the use of this disinfection technology in the oral cavity. In this direction, it becomes of critical importance to develop visible-light-driven antibacterial properties of nTiO_2.

Several approaches have been tested to re-engineer the TiO_2 band gap in order to extend the photocatalyst's light absorption into the visible range. Typically, these electronic alterations are based on chemical modifications of titania's crystal lattice by doping, ion implantation, sensitization or coupling with plasmonic noble metal nanoparticles. The doping approach, using either transition metals or non-metal ions, such as nitrogen, has attracted the majority of the scientific community's attention due to its promising results and potent antibacterial potential. The present study has offered to the field the development of an antibacterial dental adhesive resin based on the incorporation of N_TiO_2 into OptiBond Solo Plus.

The nanoparticles presented herein were obtained via a two-step fabrication process. In the first step, undoped TiO_2 nanoparticles were synthesized according to the method described by Dinh et al. [48]. Then, the second step of the fabrication process involved nitrogen-doping procedures that were carried out similarly to the methods previously published by Huo et al. [49]. After the nitrogen-doping process, the obtained nanoparticles had their initial visual aspect altered from a bright white into a yellow-pale suspension, which according to Di Valentin et al. [52] is a good indication that the doping process was carried out successfully. The results of the UV-vis spectroscopy of both undoped and N_TiO_2 are

presented in Figure 1, where it is possible to observe that N_TiO_2 samples presented higher levels of light absorption when compared to the behavior observed for undoped samples. Our findings are in agreement with the results previously reported by Peng et al. [53], who demonstrated that the modification of Titania by nitrogen, under hydrothermal conditions, resulted in the manufacturing of nanoparticles with a significant absorption behavior in the visible region (between 400 and 600 nm).

The SEM analysis of nanoparticles is presented in Figure 2. The results obtained have revealed important aspects related to nanoparticles' morphologies and agglomeration levels. The layered and amorphous structures visible in the images suggest that N_TiO_2 have spherical shapes, smooth surfaces and display a strong agglomeration behavior in ethanol (40 mg/mL). The use of surfactants is one approach that could be used in the present study to improve the dispersibility behavior of N_TiO_2. However, the use of surfactants could significantly decrease the possibility of oxidation reactions taking place on the surface of N_TiO_2 due to the creation of a physical barrier, thereby diminishing their antibacterial behavior. In this direction, our fabrication strategy was designed to maximize the photocatalytic behavior of N_TiO_2. It is also important to underscore that the agglomeration levels observed are not associated with the establishment of irreversible chemical bonds among nanoparticles. The SEM images simply demonstrate a physical association of nanoparticles due to the drying process that is required for SEM imaging. Kairyte et al. (2013) [54] while investigating the antibacterial behavior of water suspensions of ZnO nanoparticles (nZnO) against *Escherichia coli and Listeria monocytogenes*, reported remarkable antifungal activity for photoactivated nZnO and agglomeration behaviors that were similar to the behaviors observed for N_TiO_2 in the present study.

The results of the nanoparticles' compositional characterization using EDS are presented in Figure 3. The analysis revealed that Ti (40.9 %), O (39.3 %), C (13.3 %) and Si (6.5 %) were the major components found in N_TiO_2 samples. However, under the conditions of the present study, the doping element (nitrogen) could not be mapped. We believe that the combination of factors like the low atomic number of nitrogen (Z= 7), and the complete overlap between the Ti L_λ (0.395 keV) and the N K_α (0.392 KeV) peaks have obscured the mapping of nitrogen in our N_TiO_2 samples. According to Goldstein et al. [55], the characterization of light elements such as Be, B, N and F is also difficult due to their low photon energies, low yield of x-rays and low energy to noise ratio.

The results of the nanoparticles' characterization using TEM are presented in Figure 4. The images clearly demonstrated that N_TiO_2 have mostly spherical shapes, smooth surfaces and a homogeneous distribution of sizes, with individual nanoparticles sizes ranging around 10 nm. It is also possible to observe that N_TiO_2 still tend to have strong agglomeration behaviors even in very diluted samples (1:1250 or 0.032 mg/mL). Our findings related to the nanoparticles' sizes, morphologies and agglomeration behavior are further corroborated by a recent study published by Huang et al. (2015) [56], who have synthesized co-doped nitrogen-and-platinum TiO_2 through a sol-gel process at low hydrolysis temperatures (20–40°C). The nanoparticles characterized in their study were spherical in shape with sizes that varied around 10 nm. In addition, the authors observed a correlation between the levels of nanoparticles' agglomeration with the hydrolysis temperature at which the nanoparticles

were synthesized, and concluded that nanoparticles synthesized at lower hydrolysis temperatures displayed fewer agglomerates and higher photocatalytic activities, as measured by the production of H_2. In our opinion, the control of the nanoparticles' agglomeration levels is a key factor in the optimization of photocatalytic reactions because agglomeration can decrease the nanoparticles' surface to volume ratio, decrease the amount of free surface area that is actually available for oxidative reactions to take place and, most importantly, increase the amount of recombination centers present in the bulk of the photocatalyst. We believe that the combination of these factors adversely impacts the overall photocatalytic behavior of light responsive materials.

SEM and EDS analyses were used to characterize the surface properties and compositions of specimens fabricated with both unaltered and experimental dental adhesive resins. The SEM results have clearly demonstrated the successful incorporation of nanoparticles in the polymer matrix, which can be observed by the presence of increasing amounts of particulates on the surfaces of specimens that were fabricated with higher nanoparticle concentrations. In addition, specimens fabricated with higher nanoparticle content displayed rougher surfaces when compared to specimens of OptiBond Solo Plus resin due to the strong presence of exposed particulates.

The compositional analysis performed using EDS further corroborates our SEM findings regarding the successful incorporation of nanoparticles into OptiBond Solo Plus. It is possible to observe on the EDS images, that specimens of OptiBond Solo Plus displayed barium (Ba), silicon (Si), oxygen (O) and carbon (C) as its major chemical components, which is an expected composition for OptiBond Solo Plus. The compositional mapping of specimens fabricated with experimental dental adhesive resins containing 50, 67 or 80 % (v/v) of N_TiO_2 clearly demonstrated higher concentrations of Ti and O, which can be noticed by observing increasing amounts of pink (Ti) and yellow (O) dots on the images. These results seem to be in good agreement with the compositions expected for samples fabricated with experimental materials.

The measurement of contact angles was performed to investigate the impact of the incorporation of nanoparticles on the wettability characteristics of OptiBond Solo Plus. According to Namen et al. [57], the measurement of contact angles at the solid-liquid-vapor interface is considered to be the most widely known technique used to investigate the wettability of solid surfaces. They also stated that the hydrophobicity behavior of dental composites is a factor of critical importance for resin-based materials because it affects the initial absorption of water, which regulates the attachment of oral bacteria. The wettability findings reported in the present study demonstrated that the incorporation of N_TiO_2 into OptiBond Solo Plus promoted the attainment of experimental materials with wettability properties that were not significantly different when compared to the control group. From the clinical perspective, the fact that there were no statistically significant differences among the groups is of critical clinical importance because dental adhesive resins have to compete with water from the dentine substrate to wet the collagen fibrils in order to promote the establishment of an adequate adhesive layer. Furthermore, Prado et al. [58] stated that adhesive materials must come into intimate contact with the dentine substrate to allow for adequate micromechanical attachment.

The antibacterial assays performed with experimental adhesive resins containing 50, 67 or 80 % (v/v) of N_TiO_2 against *S. mutans* biofilms grown for either 3 or 24 hours, with or without continuous light irradiation, are presented in Figures 8 and 9, respectively. These results have demonstrated that, independent of growth time (either 3 or 24 hours) or light irradiation conditions (with or without light), experimental groups containing higher N_TiO_2 concentrations were more antibacterial in nature when compared to the control group, which indicates the establishment of a concentration-dependent antibacterial mechanism. In addition, it is possible to observe that specimens containing 50, 67 or 80 % (v/v) of N_TiO_2 have displayed interesting dark cytotoxicity behaviors, wherein specimens fabricated with 67% of N_TiO_2 promoted bacterial reductions in the order of 2.4 $\log_{10}$ when compared to unaltered dental adhesive resins. Such promising antibacterial behavior could be translated into novel restorative dental biomaterials with improved service lives, less incidence of failure by secondary caries and a significant decrease in oral health care costs, which are current objectives of the U.S. National Institutes of Health.

The CLSM images presented in Figure 10 illustrate and further corroborates the results of the antibacterial assays performed on dental adhesive resins. These results confirm a decrease in cells viability and biovolume when specimens were fabricated with higher concentrations of nanoparticles while also being irradiated with continuous visible light irradiation, and therefore align the expected results with the representative CLSM images. It is interesting to note, that while it was expected that the N_TiO_2 nanoparticles would affect the viability of *S. mutans* biofilms when exposed to visible light, it is apparent that there is a dark toxicity effect. Although many photocatalysts are able to increase bactericidal effects, they usually require an irradiation light source in order to elicit reduced viability [59]. However, the dark toxicity experienced in this study is shown to be statistically significant due to decrease in viability between the OptiBond Solo Plus control and the adhesives containing 50, 67 and 80 % of N_TiO_2 nanoparticles in dark conditions in both the 3 and 24-hour biofilms. It is also supported by the 24-hour CLSM images that qualitatively have shown a significant change in viability, but not necessarily the structure of the biofilm.

There are many reports on how blue light exposure reduces viability of already established biofilms [60–62]. However, de Sousa et al. [63] conducted a series of experiments to determine how blue light affects the growth of biofilms over time. They concluded that treating biofilms twice daily with blue light irradiation inhibited the extracellular polymeric substances (EPS), which prevented a stable scaffold of the extracellular biofilm matrix. Even though their CLSM images confirm that blue light prevented biofilm development, surprisingly there is still a minimal antimicrobial effect when compared to the control. Both our CLSM images as well as our CFU/mL results show not only a decrease in biovolume, but also a highly toxic effect when biofilms are grown on an adhesive containing N_TiO_2 nanoparticles in the presence of blue light. Since it has been previously established that the nanoparticles do have some degree of dark toxicity, it is acceptable to entertain the possibility that the high degree of bactericidal effects were due to a two-part mechanism; the restriction of EPS in the formation of the biofilm, as well as the toxicity of the nanoparticles themselves.

Conclusions:

In the present study, a titanium dioxide-based photocatalyst has been successfully prepared by doping TiO_2 nanoparticles with nitrogen using a simple solvothermal method. This method was demonstrated to have superior visible light absorption levels when compared to pure TiO_2 due to the contribution of substitutional nitrogen in the crystal lattice of titanium. The visible light-driven antibacterial efficacy of N_TiO_2 was investigated for nanoparticles incorporated in a commercially available dental adhesive resin. The present study has shown for the first time that specimens fabricated with experimental dental adhesive resins containing either 50, 67 or 80 % (v/v) of N_TiO_2 were shown to have strong antibacterial behavior in both, dark and light irradiated conditions, when compared to the antibacterial behavior of unaltered dental adhesive resins. This suggests that N_TiO_2 is a feasible antibacterial agent against oral cariogenic biofilms. The present study has also demonstrated that experimental materials had similar wettability behaviors when compared to the unaltered adhesive resins, which is extremely important from the clinical perspective. It is clear that further optimization of nanoparticles and materials are made necessary in order to produce dental materials capable of preventing the occurrence of secondary caries.

Acknowledgements:

The research results discussed in this publication were made possible in total or in part by funding through the award project number HR16–131, from the Oklahoma Center for the Advancement of Science and Technology. The present work was also partially funded by the Oklahoma Shared Clinical and Translational Resources grant number NIGMS U54GM104938. The synthesis and some characterization of nitrogen-doped titania nanoparticles was conducted at the Center for Nanophase Materials Science, which is a DOE Office of Science user facility.

References:

[1]. Aas JA, Paster BJ, Stokes LN, Olsen I, Dewhirst FE, Defining the normal bacterial flora of the oral cavity, Journal of clinical microbiology 43(11) (2005) 5721–32. [PubMed: 16272510]

[2]. Forssten SD, Björklund M, Ouwehand AC, Streptococcus mutans, Caries and Simulation Models, Nutrients 2(3) (2010) 290–298. [PubMed: 22254021]

[3]. Melo MAS, Guedes SFF, Xu HHK, Rodrigues LKA, Nanotechnology-based restorative materials for dental caries management, Trends in biotechnology 31(8) (2013) 10.1016/j.tibtech.2013.05.010.

[4]. Horev B, Klein MI, Hwang G, Li Y, Kim D, Koo H, Benoit DS, pH-activated nanoparticles for controlled topical delivery of farnesol to disrupt oral biofilm virulence, ACS Nano 9(3) (2015) 2390–404. [PubMed: 25661192]

[5]. Flemmig TF, Beikler T, Control of oral biofilms, Periodontology 2000 55(1) (2011) 9–15. [PubMed: 21134225]

[6]. Mjor IA, Clinical diagnosis of recurrent caries, Journal of the American Dental Association (1939) 136(10) (2005) 1426–33. [PubMed: 16255468]

[7]. Mjor IA, Toffenetti F, Secondary caries: a literature review with case reports, Quintessence international (Berlin, Germany : 1985) 31(3) (2000) 165–79.

[8]. Sakaguchi RL, Review of the current status and challenges for dental posterior restorative composites: clinical, chemistry, and physical behavior considerations. Summary of discussion from the Portland Composites Symposium (POCOS) June 17–19, 2004, Oregon Health and Science University, Portland, Oregon, Dental materials : official publication of the Academy of Dental Materials 21(1) (2005) 3–6. [PubMed: 15680996]

[9]. Healey HJ, Phillips RW, A clinical study of amalgam failures, Journal of dental research 28(5) (1949) 439–46. [PubMed: 18143324]

[10]. Fusayama T, Hosoda H, Iwamoto T, An improved self-curing acrylic restoration and comparison with silicate cement restorations, The Journal of Prosthetic Dentistry 14(3) (1964) 537–553.

[11]. Mjor IA, Moorhead JE, Dahl JE, Reasons for replacement of restorations in permanent teeth in general dental practice, International dental journal 50(6) (2000) 361–6. [PubMed: 11197194]

[12]. Bernardo M, Luis H, Martin MD, Leroux BG, Rue T, Leitao J, DeRouen TA, Survival and reasons for failure of amalgam versus composite posterior restorations placed in a randomized clinical trial, Journal of the American Dental Association (1939) 138(6) (2007) 775–83. [PubMed: 17545266]

[13]. Drummond JL, Degradation, fatigue and failure of resin dental composite materials, Journal of dental research 87(8) (2008) 710–719. [PubMed: 18650540]

[14]. Konishi N, Torii Y, Kurosaki A, Takatsuka T, Itota T, Yoshiyama M, Confocal laser scanning microscopic analysis of early plaque formed on resin composite and human enamel, Journal of oral rehabilitation 30(8) (2003) 790–5. [PubMed: 12880401]

[15]. Hahn R, Weiger R, Netuschil L, Bruch M, Microbial accumulation and vitality on different restorative materials, Dental materials : official publication of the Academy of Dental Materials 9(5) (1993) 312–6. [PubMed: 7995483]

[16]. Hansel C, Leyhausen G, Mai UE, Geurtsen W, Effects of various resin composite (co)monomers and extracts on two caries-associated micro-organisms in vitro, Journal of dental research 77(1) (1998) 60–7. [PubMed: 9437400]

[17]. Sönju T, Glantz PO, Chemical composition of salivary integuments formed in vivo on solids with some established surface characteristics, Archives of Oral Biology 20(10) (1975) 687–691. [PubMed: 127573]

[18]. Orstavik D, Orstavik J, In vitro attachment of Streptococcus sanguis to dental crown and bridge cements, Journal of oral rehabilitation 3(2) (1976) 139–44. [PubMed: 1066446]

[19]. Skjorland KK, Auger analysis of integuments formed on different dental filling materials in vivo, Acta odontologica Scandinavica 40(3) (1982) 129–34. [PubMed: 6957135]

[20]. Svanberg M, Mjor IA, Orstavik D, Mutans streptococci in plaque from margins of amalgam, composite, and glass-ionomer restorations, Journal of dental research 69(3) (1990) 861–4. [PubMed: 2109000]

[21]. Dionysopoulos D, The effect of fluoride-releasing restorative materials on inhibition of secondary caries formation, Research Review Fluoride 47(3) (2014) 258–65.

[22]. Kim H-J, Kwon T-Y, Kim K-H, Kwon S-T, Cho D-H, Son J, Long-term release of chlorhexidine from dental adhesive resin system using human serum albumin nanoparticles, Polym. Bull. 71(4) (2014) 875–886.

[23]. Patel MP, Cruchley AT, Coleman DC, Swai H, Braden M, Williams DM, A polymeric system for the intra-oral delivery of an anti-fungal agent, Biomaterials 22(17) (2001) 2319–24. [PubMed: 11511028]

[24]. Leung D, Spratt DA, Pratten J, Gulabivala K, Mordan NJ, Young AM, Chlorhexidine-releasing methacrylate dental composite materials, Biomaterials 26(34) (2005) 7145–53. [PubMed: 15955557]

[25]. Anusavice KJ, Zhang NZ, Shen C, Controlled release of chlorhexidine from UDMA-TEGDMA resin, Journal of dental research 85(10) (2006) 950–4. [PubMed: 16998139]

[26]. Imazato S, Chen J.-h., Ma S, Izutani N, Li F, Antibacterial resin monomers based on quaternary ammonium and their benefits in restorative dentistry, Japanese Dental Science Review 48(2) (2012) 115–125.

[27]. Imazato S, Imai T, Russell RR, Torii M, Ebisu S, Antibacterial activity of cured dental resin incorporating the antibacterial monomer MDPB and an adhesion-promoting monomer, Journal of biomedical materials research 39(4) (1998) 511–5. [PubMed: 9492208]

[28]. Peng JJY, Botelho MG, Matinlinna JP, Silver compounds used in dentistry for caries management: A review, Journal of dentistry 40(7) (2012) 531–541. [PubMed: 22484380]

[29]. dos Santos VE Jr, Filho AV, Ribeiro Targino A.G., Pelagio Flores MA, Galembeck A, Caldas AF Jr, Rosenblatt A, A New “Silver-Bullet” to treat caries in children – Nano Silver Fluoride: A randomised clinical trial, Journal of dentistry 42(8) (2014) 945–951. [PubMed: 24930870]

[30]. Hernández-Sierra JF, Ruiz F, Cruz Pena DC, Martínez-Gutiérrez F, Martínez AE, de Jesús Pozos Guillén A, Tapia-Pérez H, Martínez Castañón G, The antimicrobial sensitivity of Streptococcus mutans to nanoparticles of silver, zinc oxide, and gold, Nanomedicine: Nanotechnology, Biology and Medicine 4(3) (2008) 237–240.

[31]. Aydin Sevinç B, Hanley L, Antibacterial activity of dental composites containing zinc oxide nanoparticles, Journal of Biomedical Materials Research Part B: Applied Biomaterials 94B(1) (2010) 22–31.

[32]. Tavassoli Hojati S., Alaghemand H, Hamze F, Ahmadian Babaki F, Rajab-Nia R, Rezvani MB, Kaviani M, Atai M, Antibacterial, physical and mechanical properties of flowable resin composites containing zinc oxide nanoparticles, Dental Materials 29(5) (2013) 495–505. [PubMed: 23562673]

[33]. Cai Y, Titanium Dioxide Photocatalysis in Biomaterials Applications, Department of Engineering Sciences, Nanotechnology and Functional Materials, Uppsala University, Uppsala, Sweden, 2013, p. 57.

[34]. Cai Y, Stromme M, Melhus A, Engqvist H, Welch K, Photocatalytic inactivation of biofilms on bioactive dental adhesives, Journal of biomedical materials research. Part B, Applied biomaterials 102(1) (2014) 62–7.

[35]. Cai Y, Strømme M, Welch K, Photocatalytic Antibacterial Effects Are Maintained on Resin-Based TiO2 Nanocomposites after Cessation of UV Irradiation, PLoS ONE 8(10) (2013) e75929.

[36]. Cai Y, Stromme M, Zhang P, Engqvist H, Welch K, Photocatalysis induces bioactivity of an organic polymer based material, RSC Advances 4(101) (2014) 57715–57723.

[37]. Matsunaga T, Tomoda R, Nakajima T, Wake H, Photoelectrochemical sterilization of microbial cells by semiconductor powders, FEMS Microbiology Letters 29(1–2) (1985) 211–214.

[38]. Foster HA, Ditta IB, Varghese S, Steele A, Photocatalytic disinfection using titanium dioxide: spectrum and mechanism of antimicrobial activity, Applied microbiology and biotechnology 90(6) (2011) 1847–68. [PubMed: 21523480]

[39]. Miguel Pelaez NTN, Pillai Suresh C., Seery Michael K., Falaras Polycarpos, Kontos Anthanassios G., Dunlop Patrik S.M., Hamilton Jeremy W.J., Anthony Byrne J, O'Shea Kevin, Entezari Mohammad H., Dionysiou Dionysios D., A review on the visible light active titanium dioxide photocatalysts for environmental applications, Applyed Catalysis B: Environmental 125 (2012) 331–49.

[40]. Girotti AW, Mechanisms of lipid peroxidation, Journal of free radicals in biology & medicine 1(2) (1985) 87–95. [PubMed: 3915303]

[41]. Maness P-C, Smolinski S, Blake DM, Huang Z, Wolfrum EJ, Jacoby WA, Bactericidal Activity of Photocatalytic TiO(2) Reaction: toward an Understanding of Its Killing Mechanism, Applied and Environmental Microbiology 65(9) (1999) 4094–4098. [PubMed: 10473421]

[42]. Wong M-S, Chu W-C, Sun D-S, Huang H-S, Chen J-H, Tsai P-J, Lin N-T, Yu M-S, Hsu S-F, Wang S-L, Chang H-H, Visible-Light-Induced Bactericidal Activity of a Nitrogen-Doped Titanium Photocatalyst against Human Pathogens, Applied and Environmental Microbiology 72(9) (2006) 6111–6116. [PubMed: 16957236]

[43]. Musk P, Campbell R, Staples J, Moss DJ, Parsons PG, Solar and UVC-induced mutation in human cells and inhibition by deoxynucleosides, Mutation Research Letters 227(1) (1989) 25–30.

[44]. Cai YL, Stromme M and Welch K, Disinfection Kinetics and Contribution of Reactive Oxygen Species When Eliminating Bacteria with TiO2 Induced Photocatalysis., Journal of Biomaterials and Nanobiotechnology 5 (2014) 200–209.

[45]. Guidelines on limits of exposure to ultraviolet radiation of wavelengths between 180 nm and 400 nm (incoherent optical radiation), Health physics 87(2) (2004) 171–86. [PubMed: 15257218]

[46]. Asahi R, Morikawa T, Ohwaki T, Aoki K, Taga Y, Visible-Light Photocatalysis in Nitrogen-Doped Titanium Oxides, Science 293(5528) (2001) 269–271. [PubMed: 11452117]

[47]. Livraghi S, Paganini MC, Giamello E, Selloni A, Di Valentin C, Pacchioni G, Origin of Photoactivity of Nitrogen-Doped Titanium Dioxide under Visible Light, Journal of the American Chemical Society 128(49) (2006) 15666–15671. [PubMed: 17147376]

[48]. Dinh C-T, Nguyen T-D, Kleitz F, Do T-O, Shape-Controlled Synthesis of Highly Crystalline Titania Nanocrystals, ACS Nano 3(11) (2009) 3737–3743. [PubMed: 19807108]

[49]. Huo Y, Bian Z, Zhang X, Jin Y, Zhu J, Li H, Highly Active TiO2-x N x Visible Photocatalyst Prepared by N-Doping in Et3N/EtOH Fluid under Supercritical Conditions, The Journal of Physical Chemistry C 112(16) (2008) 6546–6550.

[50]. Esteban Florez FL, Hiers RD, Smart K, Kreth J, Qi F, Merritt J, Khajotia SS, Real-time assessment of Streptococcus mutans biofilm metabolism on resin composite, Dental materials : official publication of the Academy of Dental Materials 32(10) (2016) 1263–9. [PubMed: 27515531]

[51]. Khajotia SS, Smart KH, Pilula M, Thompson DM, Concurrent Quantification of Cellular and Extracellular Components of Biofilms, (82) (2013) e50639.

[52]. Di Valentin C, Finazzi E, Pacchioni G, Selloni A, Livraghi S, Paganini MC, Giamello E, N-doped TiO2: Theory and experiment, Chemical Physics 339(1–3) (2007) 44–56.

[53]. Peng F, Cai L, Huang L, Yu H, Wang H, Preparation of nitrogen-doped titanium dioxide with visible-light photocatalytic activity using a facile hydrothermal method, Journal of Physics and Chemistry of Solids 69(7) (2008) 1657–1664.

[54]. Kairyte K, Kadys A, Luksiene Z, Antibacterial and antifungal activity of photoactivated ZnO nanoparticles in suspension, Journal of Photochemistry and Photobiology B: Biology 128 (2013) 78–84.

[55]. Josheph DN, Goldenstein I, Joy David, Lyman Charles, Echlin Patrick, Lifshin Eric, Sawyer Linda, and Michael Joseph, Scanning Electron Microscopy and X-ray Microanalysis, 3rd ed., Kluwer Academic 1 Plenum Publishers2007.

[56]. Huang B-S, Tseng H-H, Su E-C, Chiu IC, Wey M-Y, Characterization and photoactivity of Pt/N-doped TiO2 synthesized through a sol–gel process at room temperature, J Nanopart Res 17(7) (2015) 1–10.

[57]. Namen F, Galan J Jr, Oliveira J.F.d., Cabreira RD, Costa e Silva Filho F, Souza AB, Deus G.d., Surface properties of dental polymers: measurements of contact angles, roughness and fluoride release, Materials Research 11 (2008) 239–243.

[58]. Prado M, de Assis DF, Gomes BP, Simao RA, Effect of disinfectant solutions on the surface free energy and wettability of filling material, Journal of endodontics 37(7) (2011) 980–2. [PubMed: 21689555]

[59]. Meisel P, Kocher T, Photodynamic therapy for periodontal diseases: state of the art, Journal of photochemistry and photobiology. B, Biology 79(2) (2005) 159–70.

[60]. Araujo NC, Fontana CR, Bagnato VS, Gerbi ME, Photodynamic effects of curcumin against cariogenic pathogens, Photomedicine and laser surgery 30(7) (2012) 393–9. [PubMed: 22693952]

[61]. Chebath-Taub D, Steinberg D, Featherstone JD, Feuerstein O, Influence of blue light on Streptococcus mutans re-organization in biofilm, Journal of photochemistry and photobiology. B, Biology 116 (2012) 75–8. [PubMed: 22982208]

[62]. Feuerstein O, Moreinos D, Steinberg D, Synergic antibacterial effect between visible light and hydrogen peroxide on Streptococcus mutans, The Journal of antimicrobial chemotherapy 57(5) (2006) 872–6. [PubMed: 16533827]

[63]. Lins de Sousa D, Araújo Lima R, Zanin IC, Klein MI, Janal MN, Duarte S, Effect of Twice-Daily Blue Light Treatment on Matrix-Rich Biofilm Development, PLoS ONE 10(7) (2015) e0131941.

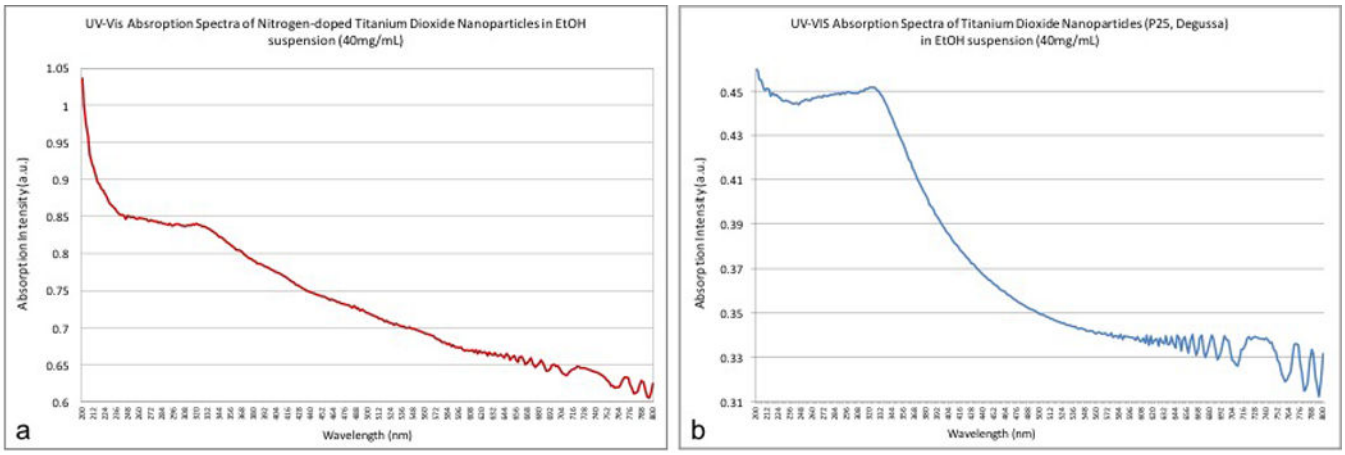

Figure 1.

Optical absorption spectrum of (a) Nitrogen-doped titanium dioxide (N_TiO_2) and (b) titanium dioxide (P25, Degussa) nanoparticles investigated. The graphs displayed have clearly illustrated that N_TiO_2 displayed higher optical absorption behavior for the range of wavelengths considered.

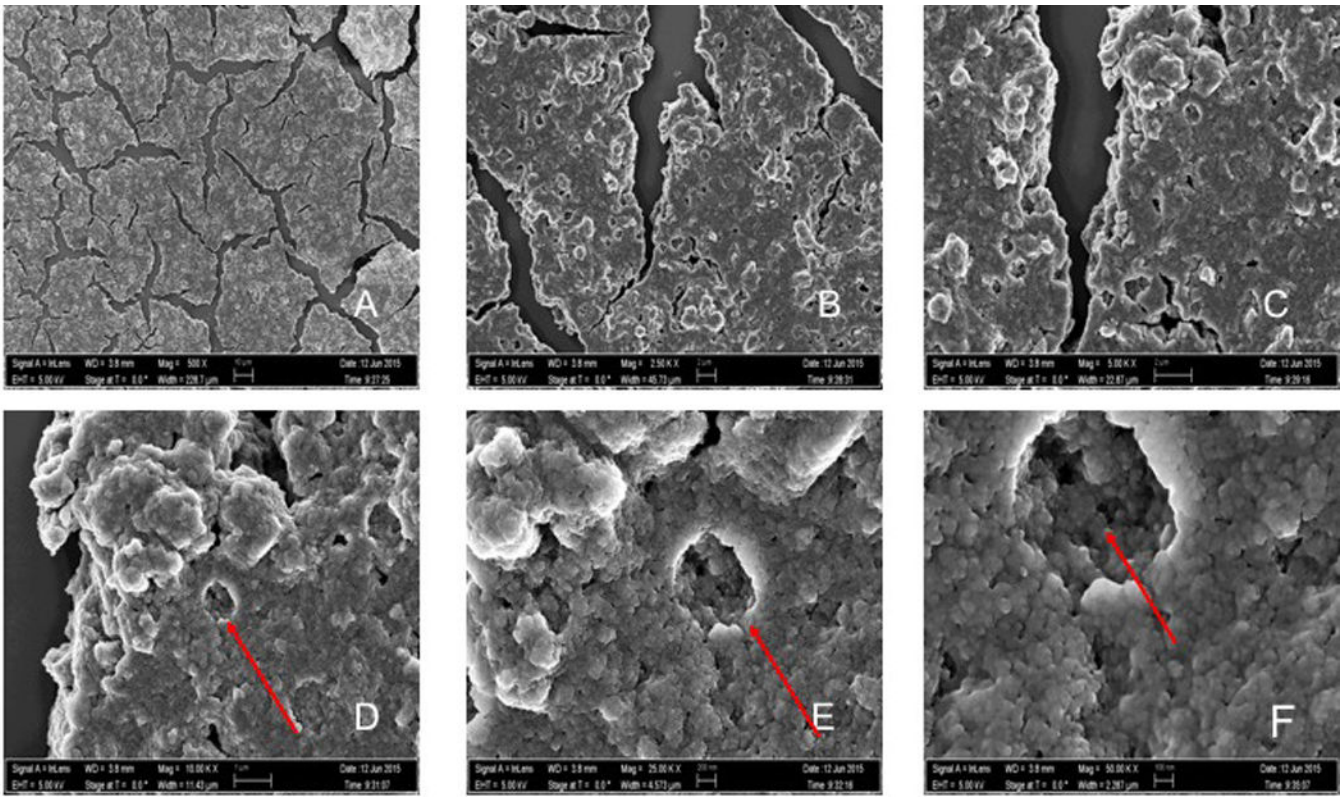

Figure 2.

SEM images demonstrating intense agglomeration of N_TiO_2 nanoparticles (40mg/mL, Oak Ridge National Laboratory, USA). Images A-F show magnifications of 500x, 2.50Kx, 5.00Kx, 10.00Kx, 25.00Kx and 50.00Kx, respectively. It is possible to observe on the images of higher magnification (D-F) that the strong agglomeration pattern promoted the formation of layered structures potentially several hundred microns thick (Z direction).

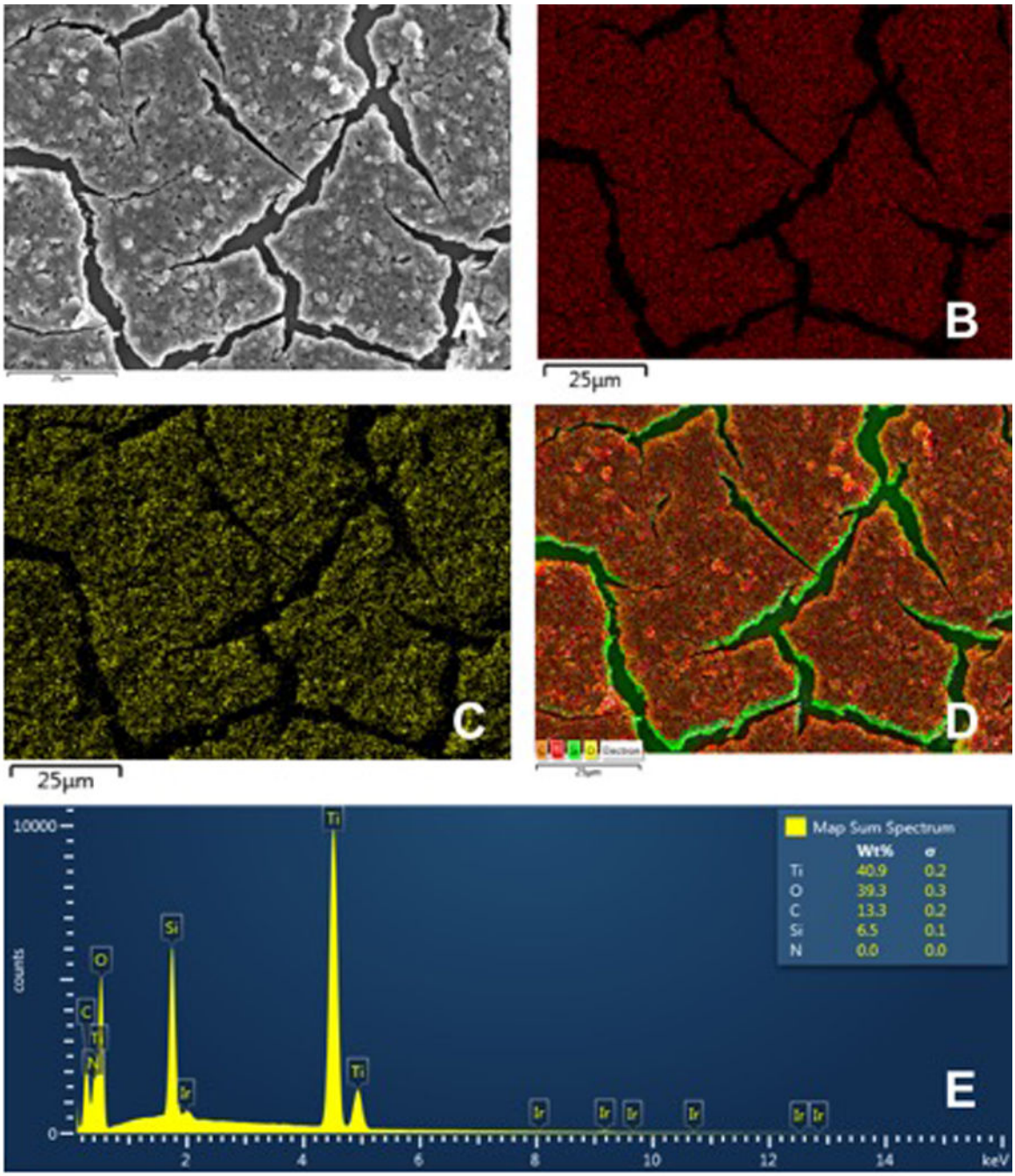

Figure 3.

Energy Dispersive X-rays Spectroscopy images. (A) Representative image of N_TiO_2 using X-Rays. (B) Mapping image of the titanium (Ti) presence in the investigated sample. (C) Mapping image of the oxygen (O) presence in the investigated sample. (D) EDS layered image demonstrating the Ti and O mapping. In the layered image, it is also possible to observe the presence of carbon and silicon. (E) Compositional analysis of the investigated sample. Visible peaks confirming the presence of elements and relative amounts in the sample investigated.

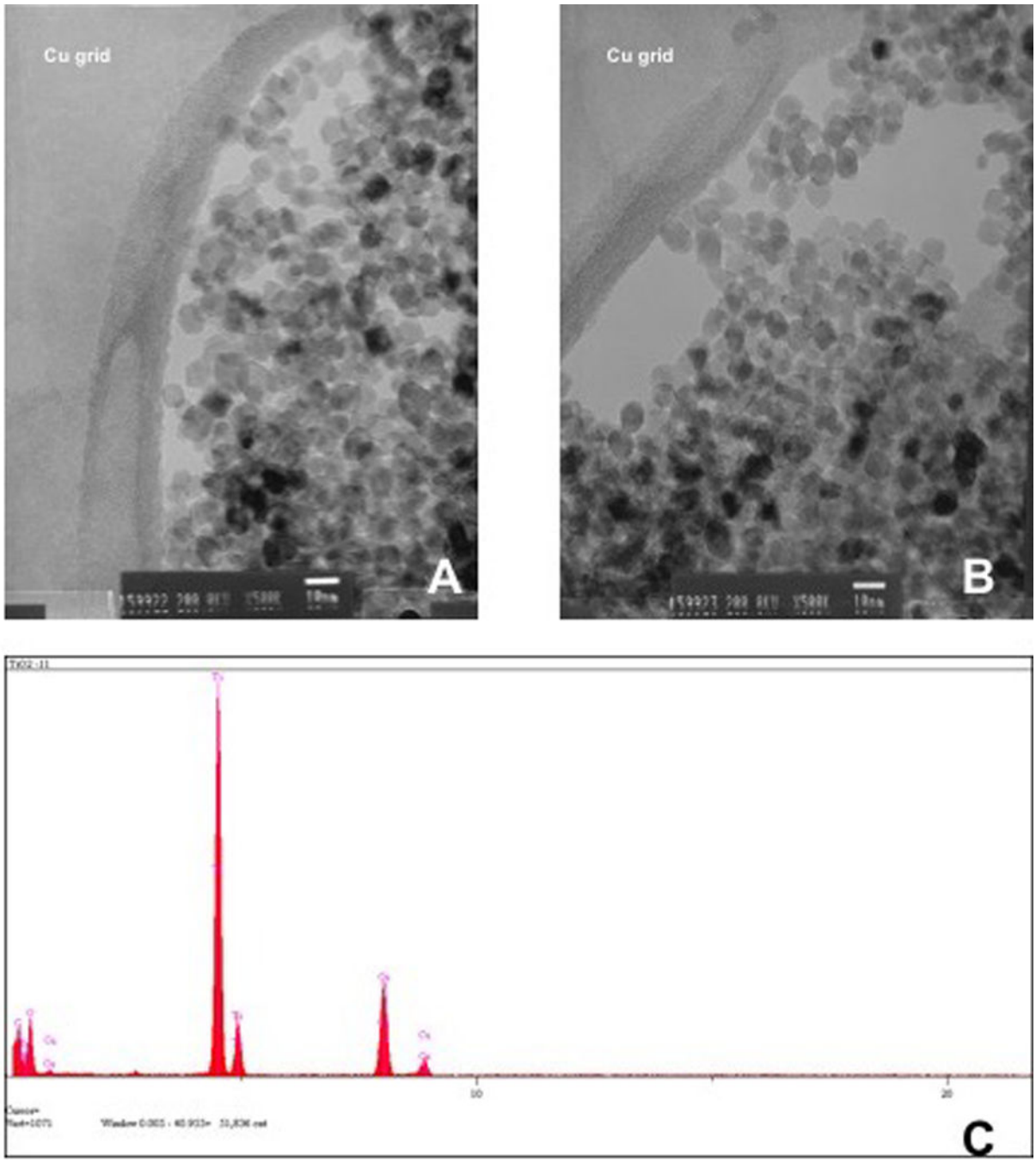

Figure 4.

TEM images (500Kx) of N_TiO_2 samples diluted in ethanol (1:1250, 200 proof). (A-B) Representative images confirming the nanoparticles' spherical shape, smooth surface and sizes around 10nm. It is also possible to observe that nanoparticles tend to aggregate even in a very diluted sample. TEM images also display the presence of the copper grid used during the images acquisition. (C) Compositional analysis performed during the TEM characterization.

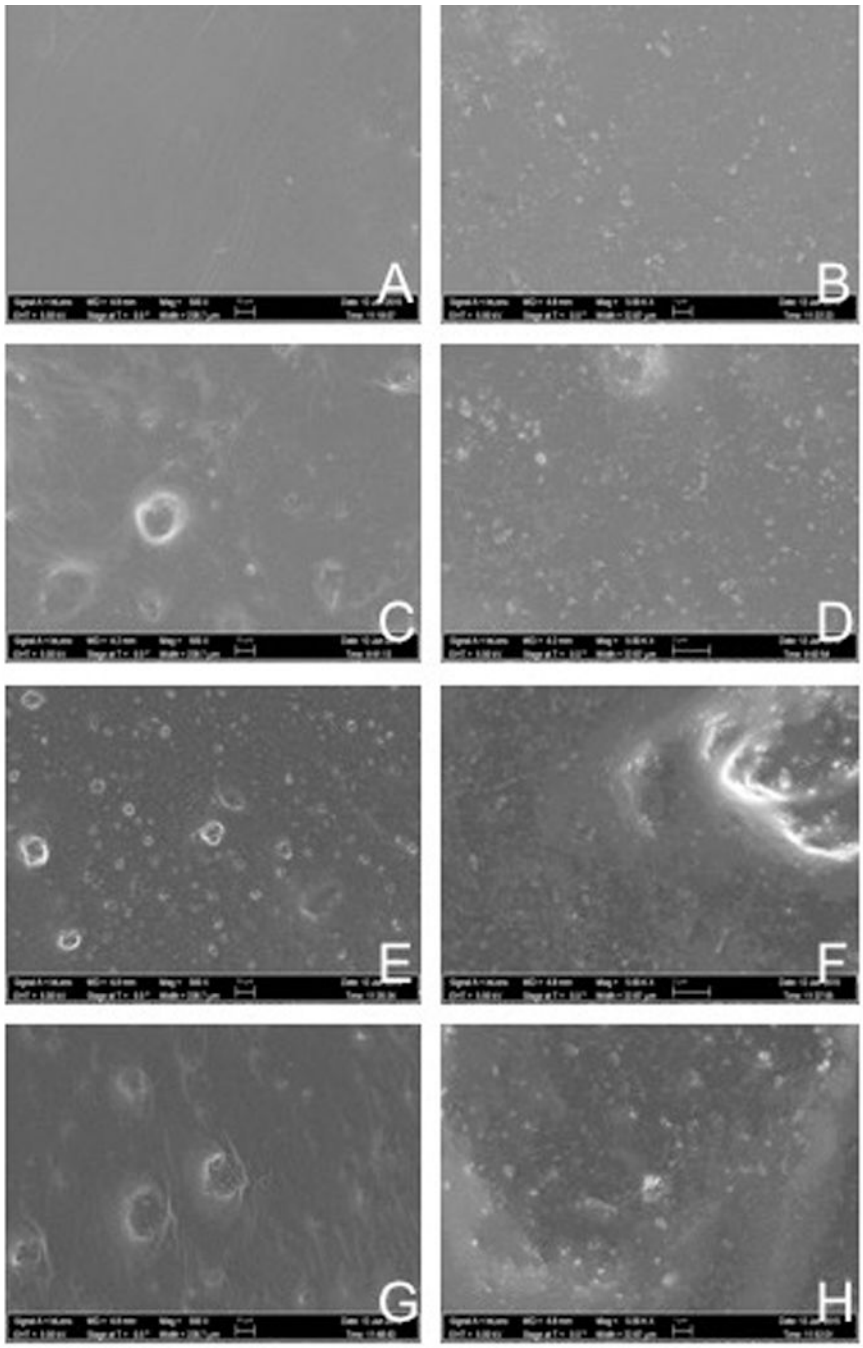

Figure 5.

SEM pictures (500x and 5,000x magnification) of thin-films (thickness≅15μm) fabricated using unaltered and experimental dental adhesive resins containing N_TiO_2 concentrations of 50, 67 and 80% (v/v). The SEM analysis confirmed the successful incorporation of N_TiO_2 in the polymer matrix by revealing the presence of increasing amounts of particles at the surface level.

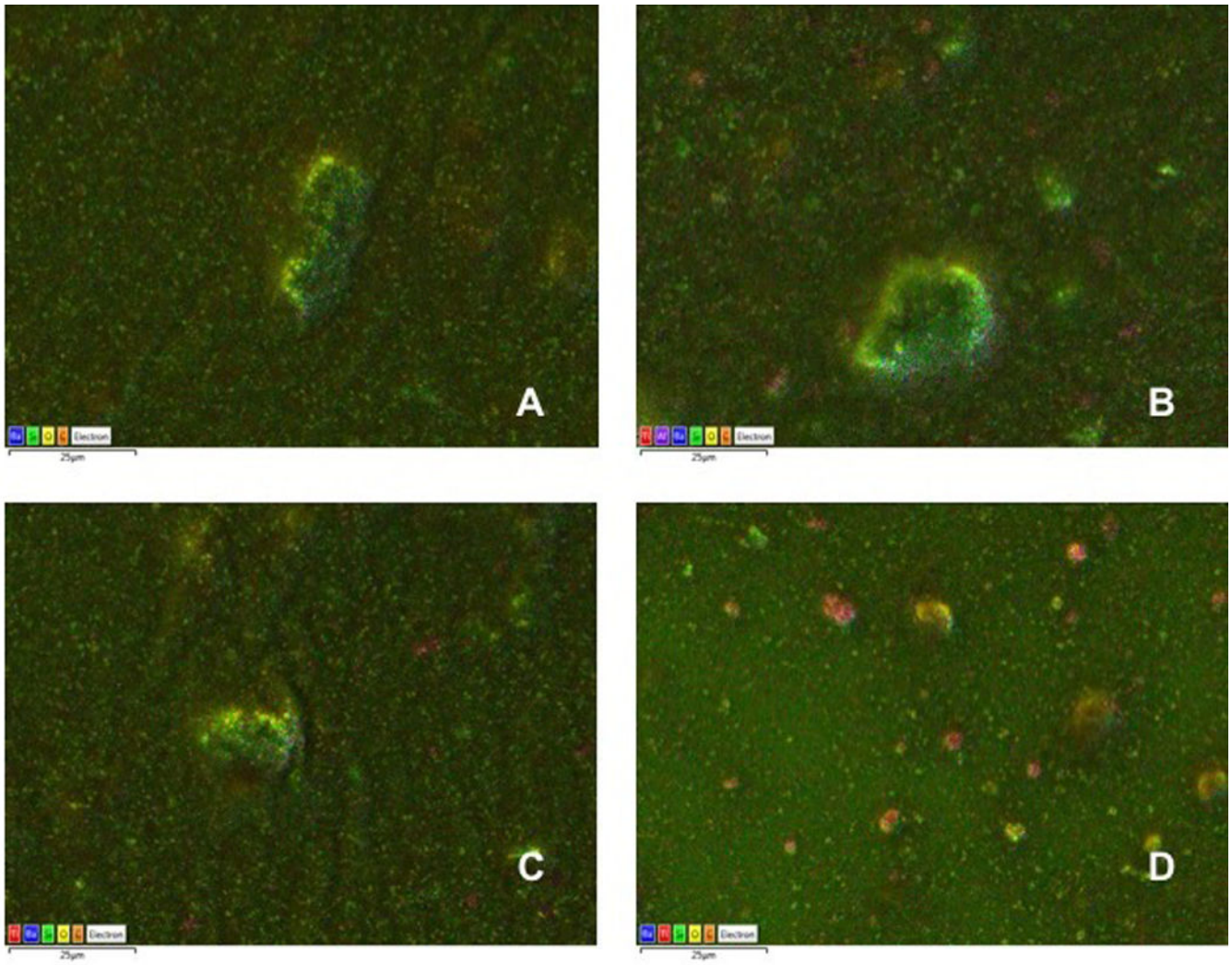

Figure 6.

EDS layered images of the elemental compositional analysis for barium (Ba), silicon (Si), oxygen (O), carbon (C), titanium (Ti) and aluminum (Al). (A) OptiBond Solo Plus, (B) Experimental adhesive resin with 50% (v/v) of N_TiO_2, (C) Experimental adhesive resin with 67% (v/v) of N_TiO_2 and (D) Experimental adhesive resins with 80% (v/v) of N_TiO_2.

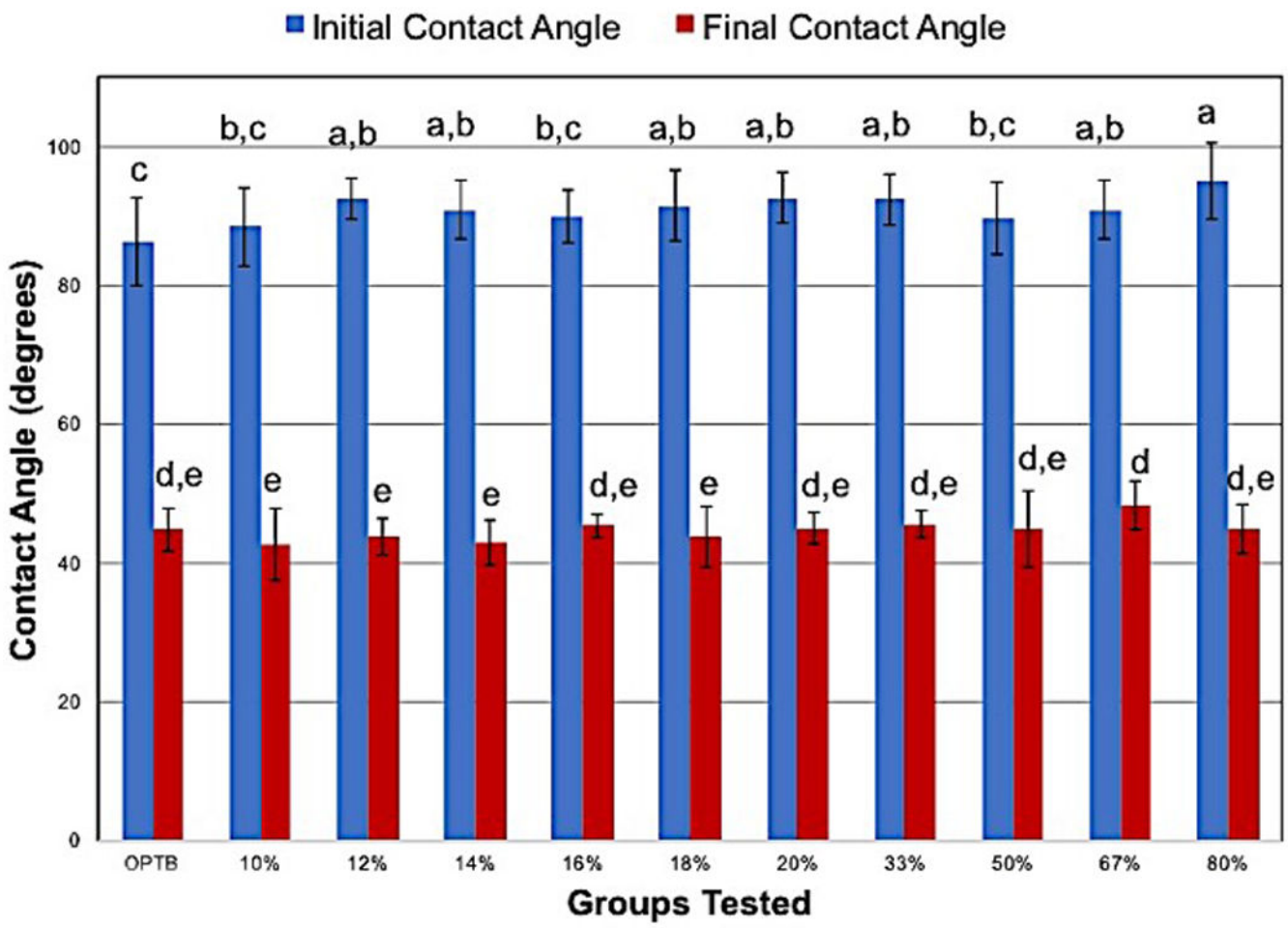

Figure 7.

Initial ($\theta_{INITIAL}$, Blue bars) and final (θ_{FINAL}, Red Bars) water wettability on dental adhesive resins at oral temperature (37°C). Different letters denote groups that present differences that were statically significant.

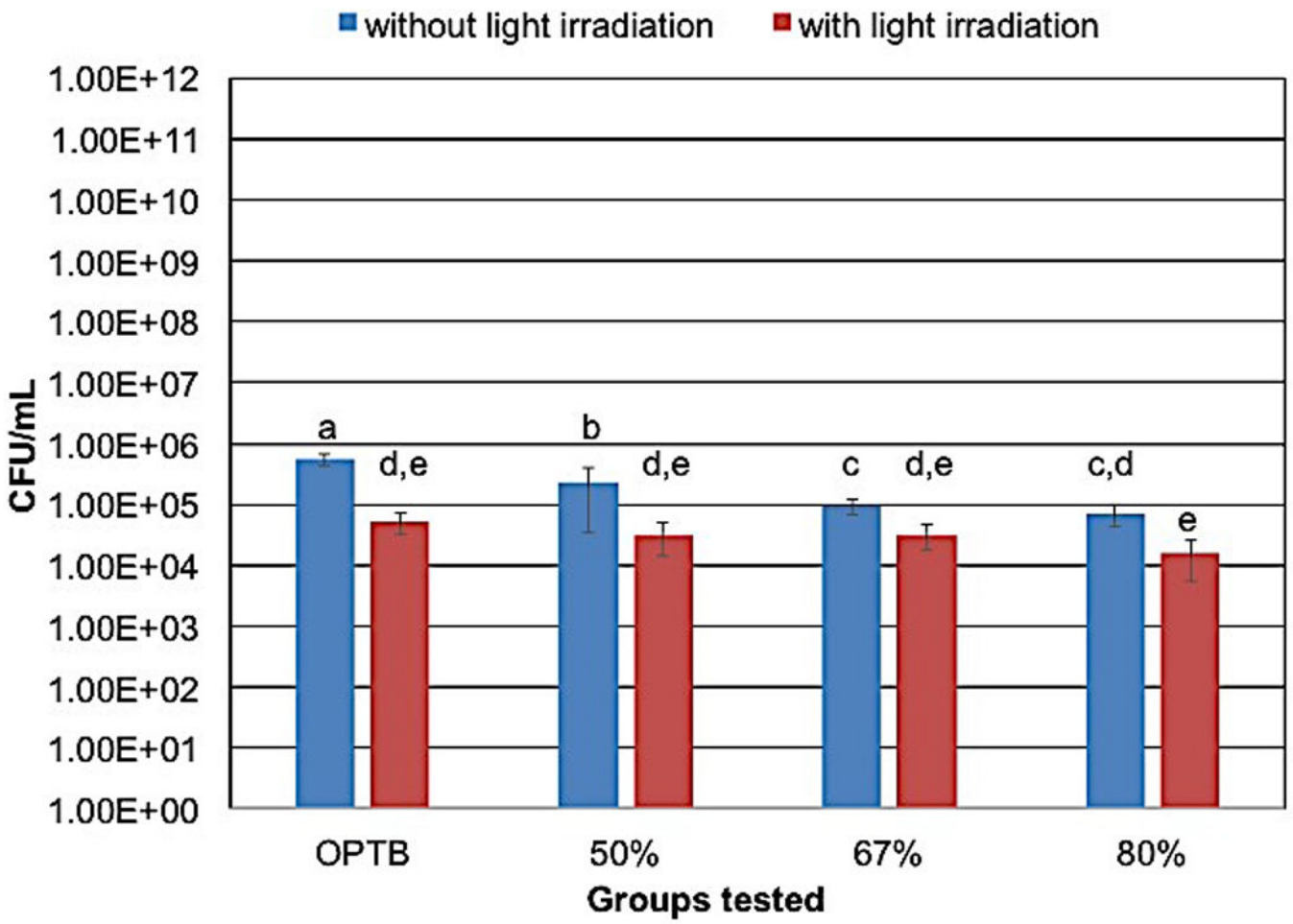

Figure 8.

Antibacterial efficacy of the groups tested. Individual columns represent mean and standard deviation values. Lower CFU/mL values indicate groups having higher antibacterial behavior.

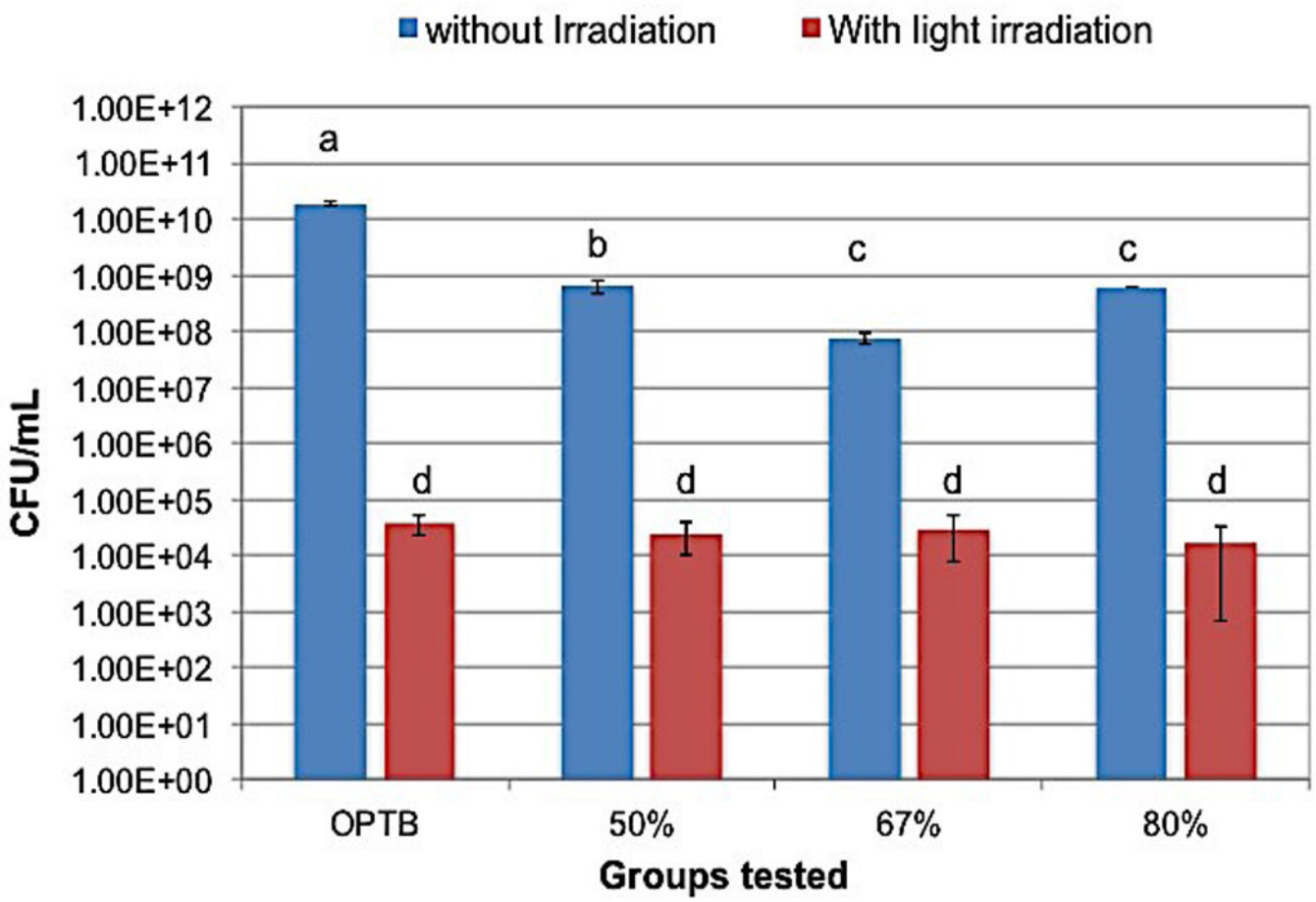

Figure 9.

S. mutans survival rate and antibacterial efficacy of the groups investigated. The survival rate (Sr) and Treatment efficacy (Te) were calculated using the following equations: $Sr=(N_f/N_0)100\%$ and $Ae=(N_0-N_f/N_0)100\%$, where N_0 is the initial population and N_f is the viable population after the treatments.

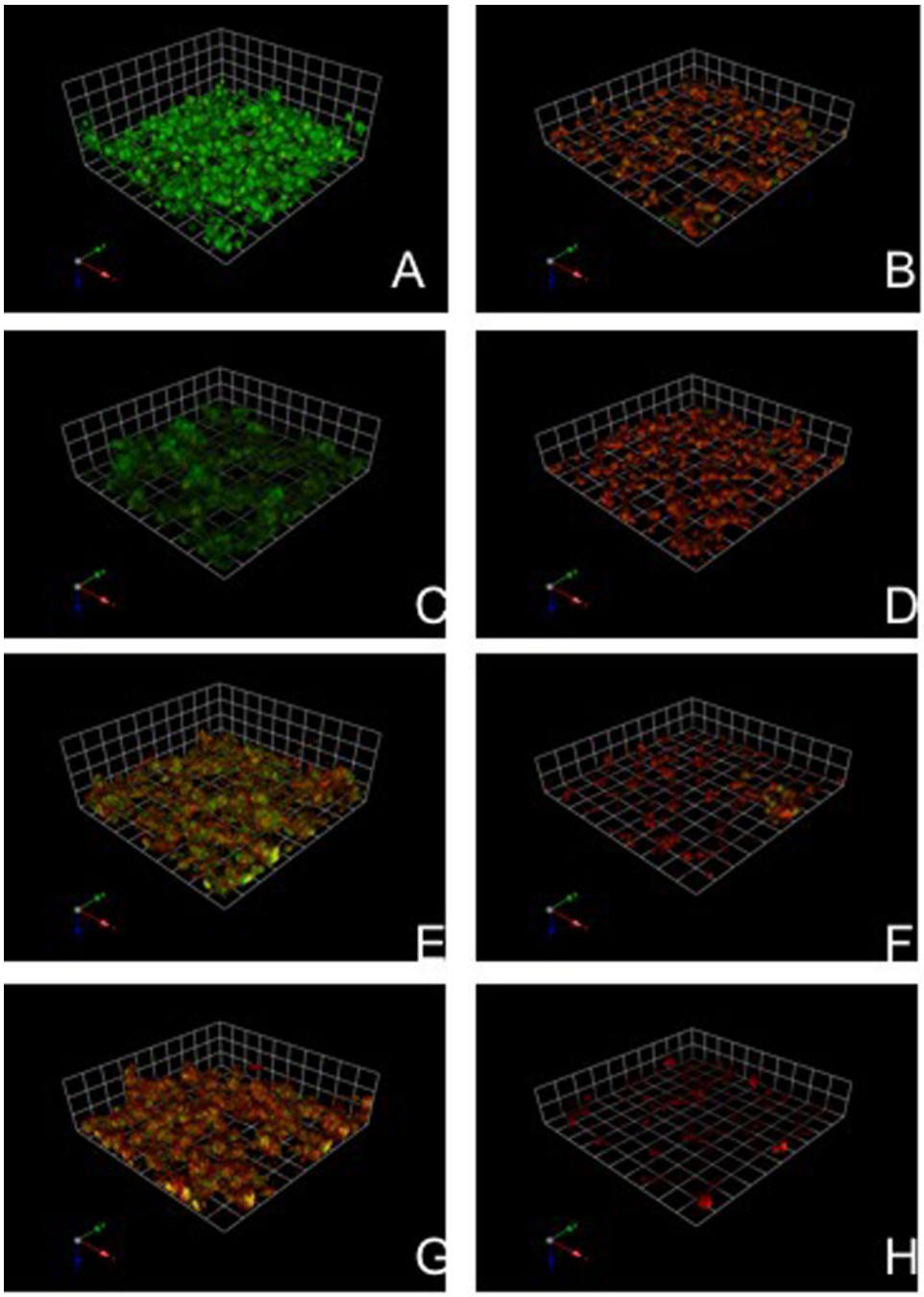

Figure 10.

Antibacterial efficacy of unaltered and experimental dental adhesive resins containing 50, 67 and 80% (v/v) of N_TiO_2 against 3-hour *S. mutans* biofilms. Individual columns represent mean and standard deviation values. Lower CFU/mL values indicate groups having higher antibacterial behavior. Distinct letters indicate groups having statistical significant differences according to the SNK *post-hoc* test.